CHEMIJA
2026. Vol. 37. No. 3. P. 217–224

ISSN 0235-7216 eISSN 2424-4538
DOI: https://doi.org/10.6001/chemija.2026.37.3.4

Adsorption properties of synthetic mayenite substituted with Si^{4+} ions

Jolanta Donėlienė,

Bartas Gedminas,

Andželika Aleinikovaitė,

Kristina Vasiliauskienė,

Anatolijus Eisinas

Department of Silicate Technology,
Kaunas University of Technology,
19 Radvilėnų Road,
50254 Kaunas, Lithuania

This work aims to determine the influence of amorphous SiO_2 on the formation of katoite, on the formation of mayenite, and on its adsorption capacity for Cu^{2+} ions. Katoite was synthesised under hydrothermal conditions (130°C; 4 h) in the primary mixture, which consisted of amorphous SiO_2, aluminium oxide and calcium oxide. It has been found that, at 350°C in the pure system, katoite completely recrystallised into a mixture of mayenite and portlandite. Moreover, in the presence of the SiO_2 additive, calcination at 350°C yielded the same products once calcium monocarboaluminate and katoite substituted with Si^{4+} ions had fully decomposed. It was also observed that MA-Si3 exhibited slightly better adsorption properties for Cu^{2+} ions than MA3: after 60 min, its adsorption capacities were 196.3 and 194.5 mg/g, respectively. It was determined that in the MA1 sample, a similar intensity of calcite, vaterite and aragonite was formed. Additionally, traces of calcium monocarboaluminate, rouaite and gibbsite were identified in the XRD patterns. Also, more intensive diffraction peaks of calcite were formed in the MA3 sample than in the MA1 and MA-Si1 samples. Moreover, higher intensity diffraction peaks characteristic of katoite formed in the MA-Si3 sample.

Keywords: mayenite, mayenite substituted with Si^{4+} ions, SiO_2, hydrothermal synthesis, adsorption

INTRODUCTION

Mayenite ($12CaO{\cdot}7Al_2O_3$ or $Ca_{12}Al_{14}O_3$) is a calcium aluminate (hydrogarnet group mineral), which can be notated by the cement system as $C_{12}A_7$ and can be found in nature [1], as a part of compounds in alumina cements [2–3] obtained via synthesis and as decomposition products of the calcium aluminate hydrate – katoite [4]. Many different synthesis techniques can be used to obtain mayenite, for example: solid-state sintering reactions [5–7], the floating zone method [8], sol–gel and subsequent calcination at high temperatures [3, 9–11], aluminothermic solid state reaction and silicothermic synthesis [9], solution combustion synthesis (SCS) [2, 12–13] and hydrothermal synthesis [4, 14].

Since different synthesis methods can be used, the choice of starting materials is also quite wide. These can be soluble salts [3, 10–12] such as calcium and aluminium nitrates and citrates, or insoluble oxides [6, 9] such as CaO, Al_2O_3 and AlOOH [15].

The $C_{12}A_7$ has a specific 3D structure where crystals have a cubic symmetry and space group values of I-43d, Z = 2, a = 11.989 Å and V = 1723.3 $Å^3$, and consists of AlO_4 tetrahedra, some of which are connected at corners and others through Ca bridges, in which Ca^{2+} has an octahedral coordination [2, 5–6]. This specific structure and a positive electric charge per unit cell, balanced by O^{2-} ions

* Corresponding author. Email: jolanta.doneliene@ktu.lt

(free oxygen ions) [16–17], lead to a quite wide field of mayenite applications. Many studies are being done to investigate its properties as the first stable electride material at room temperature [18] for use as a low-work-function field emitter [19], and conductor [20], as a catalyst [21] for ammonia synthesis, trichloroethylene oxidation [16] or for catalytic reforming of tar [22], CH_4 [23] and toluene [24], fluoride and HCl [25–26]. Also, mayenite is a frequently hydraulically active constituent of calcium aluminate cement (CAC), playing an intermediate role in the manufacture of Portland cement [3].

Environmental pollution, mainly caused by human and industrial activities, remains one of the greatest challenges of the 21st century. Water pollution by organic compounds, various pollutants and heavy metals poses a serious threat to ecosystems and living organisms. Among the various existing purification methods, adsorption, using inorganic, organic, natural and synthetic adsorbents, is widely used due to its low cost, high efficiency and simple operation. According to the literature, various adsorbents have been used to remove heavy metal ions (such as Cu [27], Pb [28], etc.) from wastewater, with extensive work on different calcium silicate hydrates [27–29]; however, research on calcium aluminate hydrates and calcium aluminates used as adsorbents is significantly less. According to some studies, due to its zeolitic structure and positive charge, mayenite is excellent at adsorbing water [6, 16] and has a good potential as a sorbent for other materials, such as heavy metals. Adsorbent materials based on mayenite can be used for cyclic carbon capture [21, 30] and in combined processes, where CO_2 adsorption/desorption is used in thermochemical energy storage systems [31–32]. The adsorption properties and the potential for widespread use are determined not only by the structure itself but also by the ability to modify it. In the late 1980s, the structure of mayenite was modified by substitution with Mn^{4+}, Mn^{2+} and Fe^{3+} ions, and its crystal structure and physicochemical properties were studied [30]. Also, some research has been conducted on properties of mayenite doped with Tb^{3+} [8, 19], P [34], Fe_2O_3 [16–17], Cu(II) [35–36], Ni [11, 37–40] and Pd/Ni [41], CeO_2 [11], LaB_6 [42], Nb [43] and others. Since the possibilities of modifying and stabilising the structure using various metal ions are most often studied, the effect of SiO_2 on the structure is no less important.

Wang et al. [7] investigated mayenite formation by precipitating $CaO–Al_2O_3–SiO_2$ melts (at 1500°C, with a starting C/A molar ratio of 1.1) and found that when the SiO_2 amount exceeded 3 wt.%, mayenite with incorporated silicon atoms in the structure formed. Meanwhile, a SiO_2 additive amount of 6 wt.% or higher inhibited mayenite formation. Azof et al. [44] determined that low concentrations of Si cations (4.7 wt.%) may stabilise the formation of $12CaO·7Al_2O_3$ at high temperatures (up to 1650°C). It works by stabilising the extra framework O^{2-} anions in $C_{12}A_7$ unit cells: Si cations impede the anions' leaving from the cages under reducing conditions and mayenite decomposition into other calcium aluminate phases. Both authors state that the $C_{12}A_7$ lattice was slightly changed due to the Si–O bond in the matrix. Since mayenite can be obtained from katoite [14], the effect of SiO_2 on katoite's structure is also important. Studying the formation of katoite during the hydration of calcium aluminate revealed that adding nanosilica alters the katoite formation: n-SiO_2 was incorporated in katoite and destabilised its phase [45].

During hydrothermal synthesis to produce katoite and mayenite, inexpensive, natural, insoluble calcined raw materials can be used, but they are often contaminated with SiO_2. Therefore, it is important to determine not only the influence of SiO_2 on the formation and stability of mayenite, but also its effects on physical and adsorption properties.

EXPERIMENTAL SECTION

Materials

Primary mixtures were prepared using CaO, γ-Al_2O_3 and amorphous $SiO_2·nH_2O$. CaO was obtained from $Ca(OH)_2$ (Sigma-Aldrich, Germany), which was calcined at 550°C for 1.5 h; the quantity of free CaO was 92 wt.%, S_a = 1341 m^2/kg (Fig. 1, curve 3). γ-Al_2O_3 was prepared by calcining $Al(OH)_3$ (Sigma-Aldrich, Germany) at 475°C for 4 h, S_a = 1129 m^2/kg (Fig. 1, curve 1). $SiO_2·nH_2O$ (Reaktiv, Russia) was ground for 2.5 min in a vibrating cup 'Pulverisette 9' mill (speed: 850 rpm), S_a = 1253 m^2/kg (Fig. 1, curve 2); the loss of ignition = 8.19 wt.%. For adsorption tests, an aqueous solution was prepared using $Cu(NO_3)_2·5H_2O$ (Sigma-Aldrich, Germany) and distilled water.

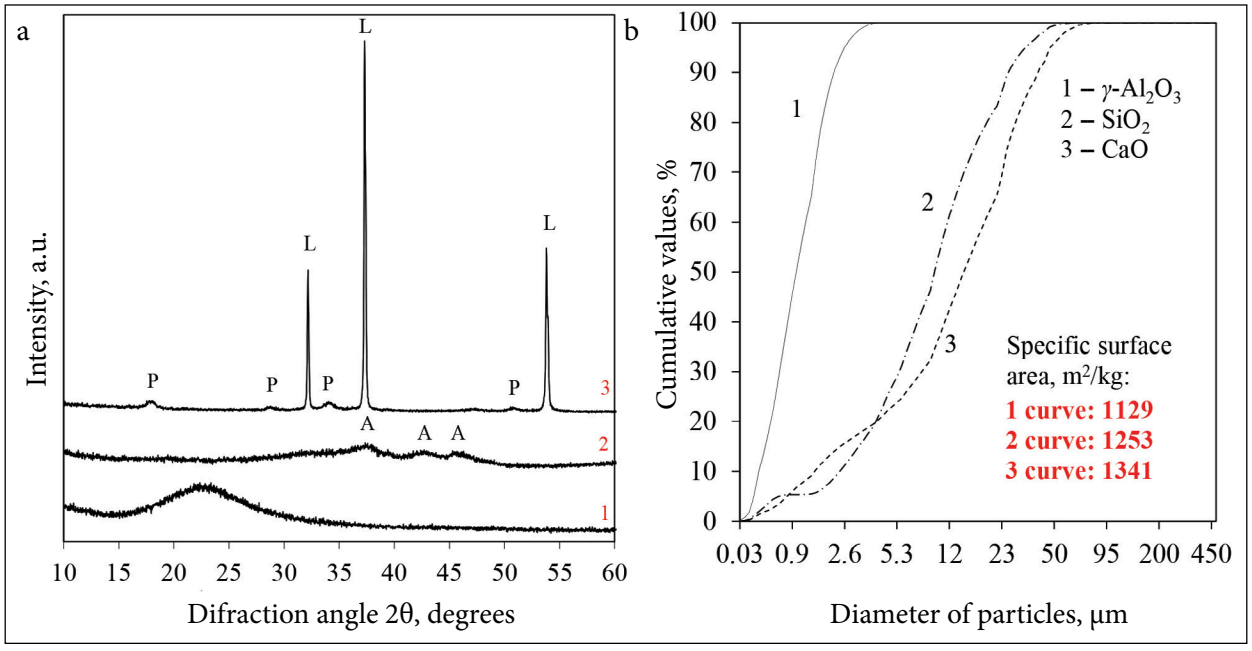

Fig. 1. XRD curves (a) and particle size distribution curves (b) of raw materials: 1, γ-Al_2O_3; 2, SiO_2·nH_2O; 3, CaO. Indexes: A, γ-Al_2O_3; S, SiO_2·nH_2O; P, portlandite; L, CaO.

Methods

The raw mixtures were prepared by mixing CaO and γ-Al_2O_3, without or with an amorphous SiO_2·nH_2O additive, in the indicated amounts. Molar ratios were CaO/(Al_2O_3+SiO_2) = 2.8 when SiO_2 = 0 or 0.25. The mixtures were homogenised for 40 min at 50 rpm in a Turbula type T2F homogeniser (Artisan Technology Group, Czech Republic). In all cases, the solution-to-solid ratio was set to 10:1. The synthesis was carried out by the hydrothermal method in PTFE cells (25 ml), which were placed in a 1 L stainless steel autoclave (Parr Instruments, Germany) under saturated steam pressure at 130°C. The isothermal condition was reached within 2 h, and the isothermal curing duration was 4 h. After the treatment, the autoclave was cooled to room temperature and the synthesis products obtained were filtered and, to prevent carbonisation, rinsed with ethanol, dried at 50 ± 5°C for 24 h, and sieved (<80 μm). Those synthesis conditions were chosen according to previously published data [4]. The samples obtained were characterised using X-ray diffraction analysis (XRD; with a Bruker D8 Advance X-ray diffractometer, tube voltage 40 kV, tube current 40 mA); simultaneous thermal analysis (STA: differential scanning calorimetry – DSC and thermogravimetry – TG, with Linseis STA PT1000 (Germany), in a temperature range of 30–1000°C, heating rate 10°C/min). The specific heat capacity (C_p) of pure mayenite and mayenite substituted with Si^{4+} ions was determined by applying a differential scanning calorimeter NETZSCH DSC 214 Polyma (Germany) when the working temperature range was 25–170°C with the constant heating rate of 10 °C/min by using Al crucibles; the flow rate of N_2 gas was 20 mL/min. The nitrogen adsorption at 77 K (S_{BET}, measured with a Quantachrome Instruments Nova) was used when the samples were degassed under vacuum at 50°C and the specific surface area of the samples was calculated by the BET equation using data from the lower part of the N_2 adsorption isotherm (0.05–0.35 p/p_0). To investigate the thermal stability of the samples, the synthesis products were calcined in a Nabertherm LH 15/13 (Germany) furnace at 350, 550 and 900°C for 1 h at a heating rate of 5°C/min. Adsorption experiments were carried out at 25°C for different time periods, varying from 3 to 60 min. 1 g of adsorbent was added to 100 mL of an aqueous $Cu(NO_3)_2$·5H_2O solution containing 2 g/L Cu^{2+} ions.

RESULTS

It was found that after 4 h of hydrothermal treatment at 130°C, synthetic katoite dominated in the pure CaO–Al_2O_3–H_2O system (Fig. 2a, curve 1). Also, traces of partially unreacted portlandite and formed calcium carbonate were observed in the XRD pattern (Fig. 2a, curve 1). It should be

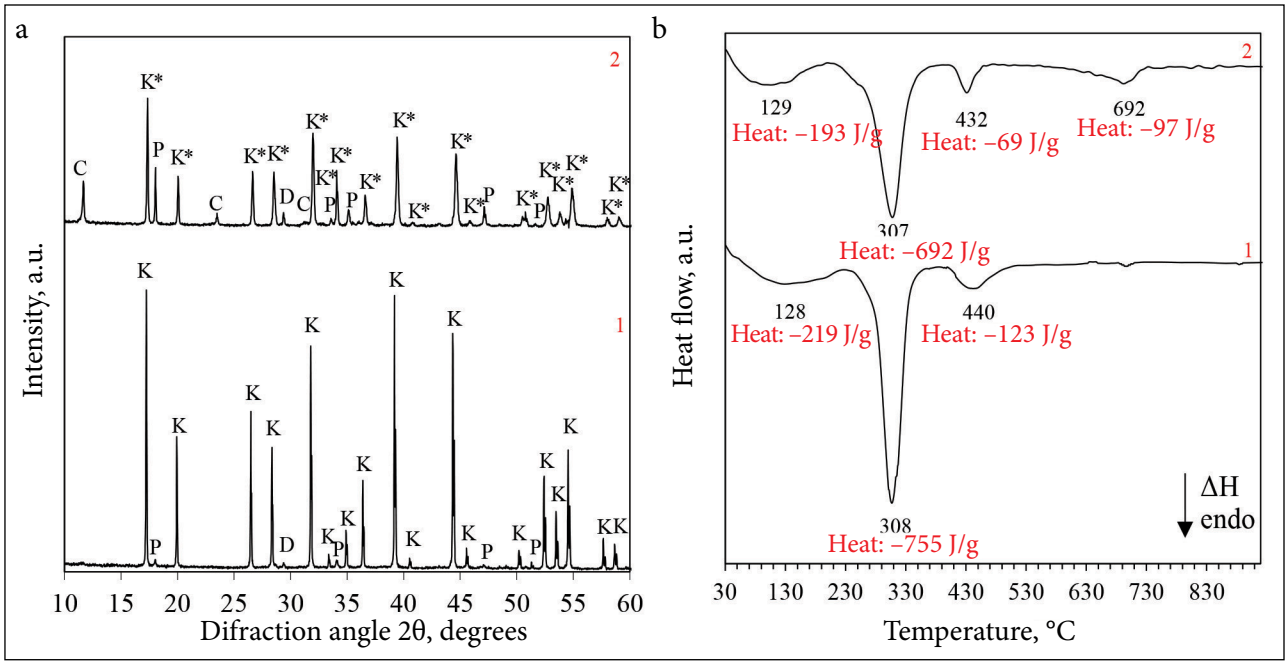

Fig. 2. XRD patterns (a) and DSC curves (b) of synthesis products when the duration of hydrothermal synthesis at 130°C is 4 h. The molar ratios of the primary mixtures were: $CaO/(Al_2O_3+SiO_2) = 2.8$; $SiO_2 = 0$ (curve 1), 0.25 (curve 2). Indexes: C, calcium monocarboaluminate ($Ca_4Al_2O_6CO_3 \cdot 11H_2O$); K, katoite ($Ca_3Al_2(OH)_{12}$); P, portlandite; D, calcite ($CaCO_3$); K*, katoite substituted with Si^{4+} ions

noted that the crystallinity of katoite increased by about 40% in the sample containing an SiO_2 additive (Fig. 2a, curve 2). Compared with the products obtained in the pure system, more intense diffraction maximum for portlandite and calcium carbonate, as well as new peaks typical of calcium monocarboaluminate, were observed (Fig. 1a, curve 2). It was determined that the amorphous SiO_2 additive became unstable and completely penetrated the product's structure because the additive's broad-reflection characteristic (Fig. 1a, curve 2) was not detected in the XRD pattern. The XRD results were confirmed by STA data: the DSC curve showed that, at ~130°C (the first endothermic effect), the amount of adsorbed heat attributed to adsorbed water of the synthesis products was 219 J/g when the products lost 0.3% of mass (in the pure system) (Fig. 2b, curve 1). Meanwhile, in the system with SiO_2 additive, the same broad endothermic peak is characteristic of dehydration of adsorbed water and the decomposition of calcium monocarboaluminate, because the heat of this endothermic effect decreased only to 193 J/g and, at the same time, the loss of mass of the synthesis products increased fourfold (1.2%) (Fig. 2b, curve 2). It was found that the decomposition of katoite (the second endothermic effect, 270–325°C) decreased from 755 J/g (in the pure system) to 692 J/g (in the system with additive) (Fig. 2b). The third endothermic peak characteristic of the decomposition of portlandite confirmed that the SiO_2 additive penetrated into the katoite structure: in the pure system, the heat of this endothermic effect was 122 J/g, and in the system with additive, it decreased to 69 J/g (Fig. 2b).

Meanwhile, the opposite results were confirmed by XRD. This phenomenon is in good agreement with the theory proposed by Rivas–Mercury et al. [46], which claims that during the dehydration of pure katoite (the second endothermic effect, 270–325°C), additional portlandite was formed, which decomposed at the same time as the primary portlandite at ~440°C temperature. Meanwhile, no additional portlandite was formed during the decomposition of katoite substituted with Si^{4+} ions. Also, the decomposition of $CaCO_3$ was observed in the 660–730°C temperature range (Fig. 2b).

In the next stage of our research, thermal stability at different temperatures (350, 550 and 900°C) of the synthetic products was performed. It was observed that at 350°C, katoite fully recrystallised to a mixture of mayenite and portlandite in the pure system (Fig. 3a, curve 1). It was also found that the synthesis products with the additive (after calcination at 350°C) formed the same products

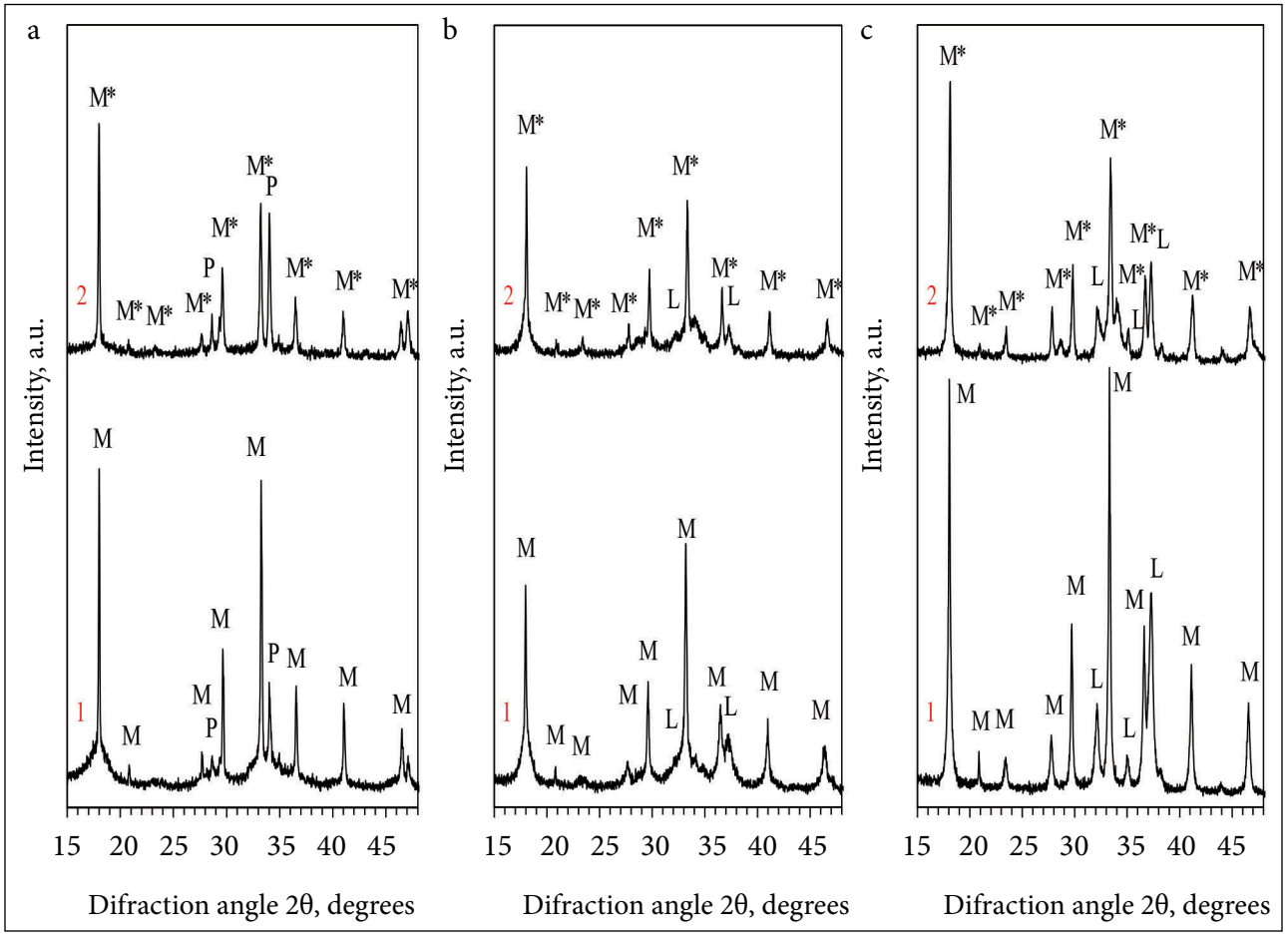

Fig. 3. XRD patterns of calcined synthesis products for 1 h (at 350°C (a), 550°C (b), 900°C (c)): in pure system (curve 1); in system with additive (curve 2). Indexes: P, portlandite; L, CaO; M, mayenite; M*, mayenite substituted with Si^{4+} ions

once the calcium monocarboaluminate and katoite, substituted with Si^{4+} ions, were fully decomposed (Fig. 3a, curve 2). The results showed that at 550°C, portlandite fully decomposed to CaO, and the intensities of the diffraction peaks of mayenite and mayenite substituted with Si^{4+} ions slightly decreased under all determined conditions (Fig. 3b). Also, when the calcination temperature increased to 900°C, the intensities of diffraction peaks characteristic of mayenite, mayenite substituted with Si^{4+} ions and CaO increased (Fig. 3c).

To evaluate the additive's influence on mayenite's physical properties, specific heat capacity (C_p) measurements were performed. Calculations showed that the heat capacity of pure mayenite samples was affected by the calcination temperature. It was determined that the lower C_p value (0.808 J/(g·K)) of mayenite was obtained after calcination at 900°C. Moreover, at 350°C, the highest specific heat capacity (0.909 J/(g·K)) was observed (Fig. 4). Also, the additive affected the mayenite

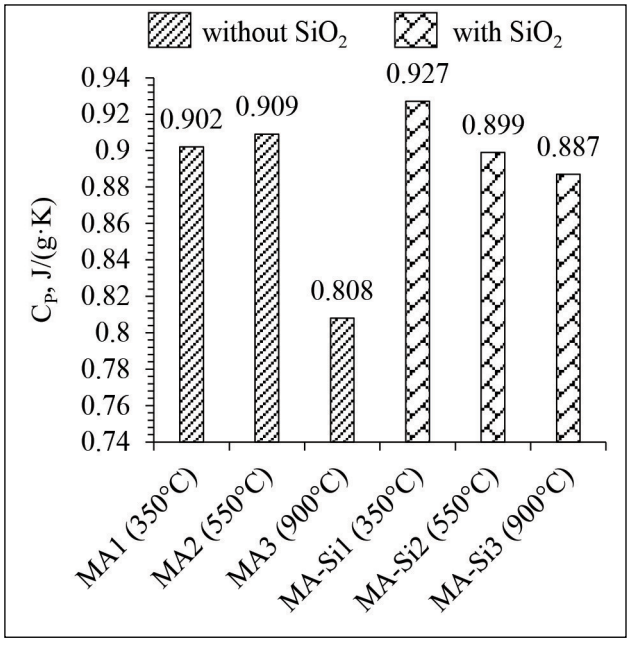

Fig. 4. The specific heat capacities (at 25°C temperature) of pure mayenite and mayenite substituted with Si^{4+} ions

specific heat capacity across all calcination temperatures. At the same time, the C_p values of mayenite substituted with Si^{4+} ions decreased slightly from 0.927 to 0.887 J/(g·K) as the calcination temperature increased (Fig. 4).

It was found that the SiO_2 additive has an influence on the synthetic samples specific surface area (Table 1). The measurements showed that the specific surface area (S_{BET}) was equal to 9.42 m^2/g, and the total pore volume was equal to 34 mm^3/g of the pure katoite sample. Meanwhile, in the system with the SiO_2 additive, the S_{BET} value slightly decreased (8.67 m^2/g), and at the same time, the total pore volume increased to 44 mm^3/g. It was determined that after calcination at a temperature of 350°C, the S_{BET} values of pure mayenite (11.21 m^2/g) and mayenite substituted with Si^{4+} ions (10.15 m^2/g) were very close. It was noted that after calcination at 550°C, the S_{BET} value in the pure system slightly decreased (9.97 m^2/g), while in the system with the additive, the specific surface area significantly decreased to 6.28 m^2/g. It was investigated that the highest S_{BET} and total pore volume values were obtained in a pure mayenite sample that was calcined at 900°C. However, these values are approximately 2 times lower than those determined in mayenite substituted with Si^{4+} ions (10.58 m^2/g; 49 mm^3/g) (Table 1).

In the next stage of research, the experiment on Cu^{2+} ions adsorption using pure mayenite (MA1; MA3) and mayenite substituted with Si^{4+} ions (MA-Si1; MA-Si3) samples with the largest specific surface area was conducted. It was found that after 3 min of the adsorption process, the amount of adsorbed copper ions by the MA1 sample was equal to 185.3 mg Cu^{2+}/g (more than 92% of copper ions were adsorbed), and after 60 min, 190.4 mg Cu^{2+} ions were adsorbed when the initial copper ions solution concentration was equal to 2000 mg/l (Table 2).

Table 2. **Adsorbed amount of Cu^{2+} ions when the initial Cu^{2+} ions concentration was 2000 mg/l**

Sample	Adsorption duration, min		
	3	20	60
	The amount of adsorbed Cu^{2+} ions, mg/g		
MA1 (350°C)	185.3	188.4	190.4
MA3 (900°C)	189.3	193.4	194.5
MA-Si1 (350°C)	186.8	189.9	191.8
MA-Si3 (900°C)	194.6	195.5	196.3

Compared with MA1, the MA-Si1 sample has a similar adsorption capacity for copper ions: at 3 min, 186.8 mg/g; after 60 min, 191.8 mg/g of copper ions were adsorbed. It was also observed that MA-Si3 exhibited slightly better adsorption properties for Cu^{2+} ions than MA3: after 60 min, its adsorption capacities were 196.3 and 194.5 mg/g, respectively.

It was determined that after the adsorption process, samples dominated by different calcium carbonate forms were observed (Fig. 5). It was determined that in the MA1 sample, a similar intensity of calcite, vaterite and aragonite was formed (Fig. 5a, curve 1).

Additionally, traces of calcium monocarboaluminate, rouaite and gibbsite were identified in the XRD patterns. The results demonstrated that lower intensity diffraction peaks of aragonite and twice as intense diffraction peaks of calcite were identified in the MA-Si1 sample. At the same time, the typical basal reflections of calcium monocarboaluminate and gibbsite were not detected in the MA-Si1 sam-

Table 1. **Samples' specific surface area (S_{BET}) and pore volume**

Sample	S_{BET}, m^2/g	C_{BET}, constant	Reliability coefficient, R^2	Pore volume, mm^3/g
Pure katoite	9.42	117.88	0.9999	34
MA1 (350°C)	11.21	139.55	0.9998	30
MA2 (550°C)	9.97	191.81	0.9996	29
MA3 (900°C)	23.34	161.14	0.9998	100
Katoite-Si	8.67	48.40	0.9999	44
MA-Si1 (350°C)	10.15	17.75	0.9996	31
MA-Si2 (550°C)	6.28	58.40	0.9999	18
MA-Si3 (900°C)	10.58	32.26	0.9999	49

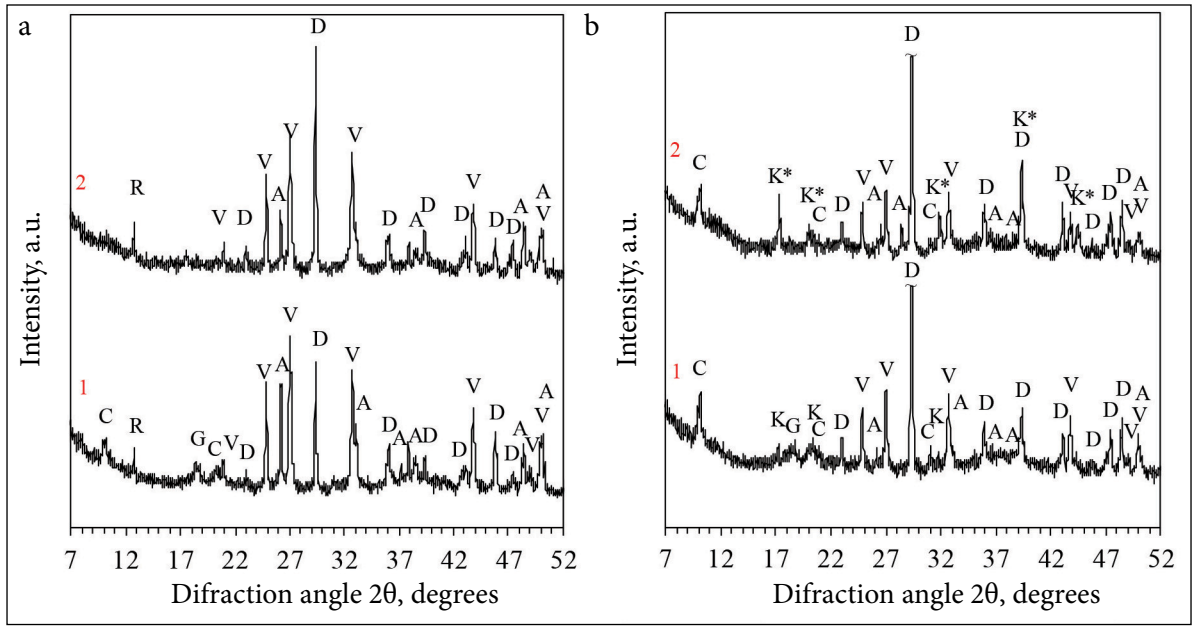

Fig. 5. XRD patterns of adsorbents after the adsorption process, obtained after calcination at 350°C (a) and 900°C (b) for 1 h (molar ratios of primary mixtures: $CaO/(Al_2O_3+SiO_2) = 2.8$; $SiO_2 = 0$ (curve 1) and 0.25 (curve 2)). Adsorbents: (a) 1, MA1; 2, MA-Si1; (b) 1, MA3; 2, MA-Si3. Indexes: C, calcium monocarboaluminate ($Ca_4Al_2O_6CO_3{\cdot}11H_2O$); D, calcite ($CaCO_3$); A, aragonite ($CaCO_3$); V, vaterite ($CaCO_3$); R, rouaite ($Cu(NO_3)(OH)_3$); G, gibbsite; K, katoite ($Ca_3Al_2(OH)_{12}$); K*, katoite substituted with Si^{4+} ions

ple (Fig. 5a, curve 2). It was determined that more intensive diffraction peaks of calcite were formed in the MA3 sample than in the samples MA1 and MA-Si1. Moreover, a new compound – katoite – was observed in X-ray diffraction patterns (Fig. 5b, curve 1). Also, more intensive diffraction peaks characteristic of katoite were observed in the XRD patterns of the MA-Si3 sample (Fig. 5b, curve 2).

CONCLUSIONS

It was observed that, after 4 h of hydrothermal treatment at 130°C in the pure $CaO–Al_2O_3–H_2O$ system, synthetic katoite became the predominant phase, accompanied by small amounts of partially unreacted portlandite and newly formed calcium carbonate. Notably, the amorphous SiO_2 additive proved unstable and was fully incorporated into the katoite structure. In comparison with the products formed in the pure system, additional diffraction peaks characteristic of calcium monocarboaluminate also appeared.

It has been found that, at 350°C in the pure system, katoite completely recrystallised into a mixture of mayenite and portlandite. It was further determined that, in the presence of the additive, calcination at 350°C yielded the same products once calcium monocarboaluminate and katoite substituted with Si^{4+} ions had fully decomposed. In addition, when the calcination temperature was increased to 900°C, the diffraction peak intensities associated with mayenite, mayenite substituted with Si^{4+} ions and CaO increased.

It was investigated that the highest S_{BET} and total pore volume values were obtained in a pure mayenite sample that was calcined at 900°C. However, these values are approximately 2 times lower than those determined in mayenite substituted with Si^{4+} ions. It was also observed that MA-Si3 exhibited slightly better adsorption properties for Cu^{2+} ions than MA3: after 60 min, its adsorption capacities were 196.3 and 194.5 mg/g, respectively.

It was determined that in the MA1 sample, a similar intensity of calcite, vaterite and aragonite was formed. Additionally, traces of calcium monocarboaluminate, rouaite and gibbsite were identified in the XRD patterns. Also, more intensive diffraction peaks of calcite were formed in the MA3 sample, than in the samples MA1 and MA-Si1. Moreover, higher intensity diffraction peaks characteristic of katoite were formed in the MA-Si3 sample.

Received 13 July 2026
Accepted 22 July 2026

References

1. E. Galuskin, I. Galuskina, Y. Vapnik, M. Murashko, *Minerals*, **10(6)**, 560 (2020).
2. I. Meza-Trujillo, F. Devred, E. M. Gaigneaux, *Mater. Res. Bull.*, **119**, 1 (2019).
3. A. A. Amer, H. El-Didamony, T. M. El-Sokkary, M. I. Wahdan, *Bol. Soc. Esp. Cer. V.*, **61(2)**, 98 (2022).
4. A. Eisinas, K. Ruginyte, K. Baltakys, et al., *Ceram. Int.*, **46(18)**, 29429 (2020).
5. M. Ruszak, S. Witkowski, P. Pietrzyk, A. Kotarba, Z. Sojka, *Funct. Mater. Lett.*, **4(2)**, 183 (2011).
6. F. I. Azof, K. Tang, J. You, J. Safarian, *Metall. Mater. Trans. B*, **51(6)**, 2689 (2020).
7. W. Wang, D. Cai, L. Zhang, I. Sohn, R. Zhao, W. Liu, *Metall. Mater. Trans. B*, **54(1)**, 221 (2023).
8. N. Kumamoto, D. Nakauchi, T. Kato, et al., *J. Rare Earths*, **35(10)**, 957 (2017).
9. V. N. Phaneuf, Ph. D. Thesis, Clemson University, South Carolina (2021).
10. B. Eryildirim, N. Oktar, D. Doğu, *Turk. J. Chem.*, **49(4)**, 479 (2025).
11. L. M. Vieira, D. B. Lima Santos, C. E. Hori, *Int. J. Hydrogen Energy*, **47(91)**, 38556 (2022).
12. F. A. Lucca Sánchez, W. Lopes de Almeida, V. Caldas de Sousa, *Ceram. Int.*, **49(10)**, 15726 (2023).
13. B. Matović, M. Prekajskia, J. Pantić, et al., *J. Eur. Ceram. Soc.*, **36(16)**, 4237 (2016).
14. C. Li, D. Hirabayashi, K. Suzuki, *Mater. Res. Bull.*, **46(8)**, 1307 (2011).
15. K. Berent, S. Komarek, R. Lach, W. Pyda, *Mater.*, **12(21)**, 3476 (2019).
16. R. Cucciniello, A. Intiso, T. Siciliano, et al., *Catalysts*, **9(9)**, 1 (2019).
17. C. Ruttanapun, P. Srepusharawoot, S. Maensiri, *Chin. J. Phys.*, **56(1)**, 252 (2018).
18. Z. Yu, Q. Liu, R. Ragipani, B. Wang, *J. Phys. Chem. C*, **124(20)**, 11150 (2020).
19. R. K. Verma, G. Kaur, A. Rai, S. B. Rai, *Mater. Res. Bull.*, **47(11)**, 3726 (2012).
20. X. Deng, J. Xu, *Ionics*, **31**, 7615 (2025).
21. A. Di Giuliano, F. Giancaterino, K. Gallucci, P. U. Foscolo, C. Courson, *Int. J. Hydrogen Energy*, **43,** 21279 (2018).
22. A. Di Carlo, D. Borello, M. Sisinni, et al., *Int. J. Hydrogen Energy*, **40(30)**, 9088 (2015).
23. S. Scaccia, L. Della Seta, D. Mirabile Gattia, G. Vanga, *J. CO_2 Util.*, **45**, 101447 (2021).
24. C. Ordóñez, I. Martínez, R. Murillo, *Appl. Catal. A Gen.*, **700**, 120266 (2025).
25. J. Ni, D. Ma, Y. X. Zhang, Y. Jia, *J. Mol. Struct.*, **1320**, 139771 (2025).
26. Y. Jia Y. Wang, C. Jiang, et al., *Energy*, **244**, 123067 (2022).
27. A. Eisinas, T. Dambrauskas, *Ceram. Int.*, **49(9)**, 14886 (2023).
28. S. Liu, S. Cui, H. Guo, Y. Wang, Y. Zheng, *Mater.*, **14(4)**, 842 (2021).
29. Q. Liu, W. Lu, W. Liu, et al., *Ceram. Int.*, **52(15)**, 29123 (2026).
30. Y. Q. Geng, Y. X. Guo, B. Fan, F. Q. Cheng, H. G. Cheng, *J. Fuel Chem. Technol.,* **49(7)**, 998 (2021).
31. R. Anwar, A. Al Kape, M. Lusi, et al., *J. Energy Storage*, **114**, 115784 (2025).
32. A. Spadoni, S. Sau, N. Corsaro, et al., *J. Energy Storage*, **72**, 108386 (2023).
33. R. Stößer, M. Nofz, W. Gesner, C. H. Schrgter, G. Kranz, *J. Solid State Chem.*, **81**, 152 (1989).
34. H. Yan Yu, X. Lin Pan, K. Wei Dong, Y. Wu, *Trans. Nonferrous Met. Soc. China*, **29(3)**, 650 (2019).
35. I. Meza-Trujillo, A. Mary, P. Pietrzyk, Z. Sojka, E. M. Gaigneaux, *Appl. Catal. B*, **316**, 121604 (2022).
36. A. Westbye, A. Aranda, P. D. C. Dietzel, L. Di Felice, *Int. J. Hydrogen Energy*, **44(25)**, 12604 (2019).
37. G. Vanga, D. M. Gattia, S. Stendardo, S. Scaccia, *Ceram. Int.*, **45(6)**, 7594 (2019).
38. A. Di Giuliano, K. Gallucci, P. U. Foscolo, C. Courson, *Int. J. Hydrogen Energy*, **44(13)**, 6461 (2019).
39. A. Di Giuliano, F. Giancaterino, C. Courson, P. U. Foscolo, K. Gallucci, *Fuel*, **234**, 687 (2018).
40. C. Ordóñez, I. Martínez, M. S. Callén, J. M. López, R. Murillo, *Fuel*, **424**, 139315 (2026).
41. C. Dang, H. Xia, S. Yuan, X. Wei, W. Cai, *Renew. Energy*, **201**, 314 (2022).
42. Q. Rong, X. Zhang, L. Yan, et al., *Ceram. Int.*, **51(7)**, 8269 (2025).
43. N. L. Kotschote, N. M. Bauer, P. J. Klar, S. G. Ebbinghaus, *J. Phys. Chem. Solids*, **213**, 113602 (2026).
44. F. I. Azof, K. Tang, J. You, J. Safarian, *Metall. Mater. Trans. B*, **51(6)**, 2689 (2020).
45. A. Solanki, L. P. Singh, S. R. Karade, U. Sharma, *Constr. Build. Mater.*, **340**, 127707 (2022).
46. J. M. Rivas-Mercury, P. Pena, A. H. Aza, X. Turrillas, *J. Eur. Ceram. Soc.*, **28(9)**, 1737 (2008).

Jolanta Donėlienė, Bartas Gedminas, Andželika Aleinikovaitė, Kristina Vasiliauskienė, Anatolijus Eisinas

SINTETINIO MAJENITO, PAKEISTO Si^{4+} JONAIS, ADSORBCIJOS SAVYBĖS